CHEMISTRY
A EUROPEAN JOURNAL

ChemPubSoc
Europe

DOI: 10.1002/chem.201202742

Tetrathiafulvalene–Benzothiadiazoles as Redox-Tunable Donor–Acceptor Systems: Synthesis and Photophysical Study

Flavia Pop,[a] Anneliese Amacher,[b] Narcis Avarvari,*[a] Jie Ding,[c] Latevi Max Lawson Daku,[c] Andreas Hauser,*[c] Marius Koch,[c] Jürg Hauser,[b] Shi-Xia Liu,*[b] and Silvio Decurtins[b]

In memory of Nuria Gallego-Planas

Abstract: Electrochemical and photophysical analysis of new donor–acceptor systems **2** and **3**, in which a benzothiadiazole (BTD) unit is covalently linked to a tetrathiafulvalene (TTF) core, have verified that the lowest excited state can be ascribed to an intramolecular-charge-transfer (ICT) π-(TTF)→π*(benzothiadiazole) transition. Owing to better overlap of the HOMO and LUMO in the fused scaffold of compound **3**, the intensity of the ^{1}ICT band is substantially higher compared to that in compound **2**. The corresponding CT fluorescence is also observed in both cases. The radical cation $TTF^{+\bullet}$ is easily observed through chemical and electrochemical oxidation by performing steady-state absorption experiments. Interestingly, compound **2** is photo-oxidized under aerobic conditions.

Keywords: charge transfer · donor–acceptor systems · fluorescence · photophysics · redox chemistry

Introduction

Intramolecular-charge-transfer (ICT) states can be useful for the design of low-energy-gap optical or electronic functional materials based on organic molecules.[1] In this respect, covalently linked donor–acceptor (D–A) systems that contain a tetrathiafulvalene (TTF)[2] derivative as an electron donor have been investigated for potential applications in various fields, such as molecular (opto)electronics, photovoltaics, and nonlinear optics.[3] It is well-known that TTF is a strong π donor that can be reversibly transformed into its radical cation ($TTF^{+\bullet}$) and dication (TTF^{2+}) through oxidation at easily accessible potentials, each of which are easily identifiable by distinct electronic absorption bands.[4] Accordingly, functional molecules and supramolecular systems that contain TTF units have been widely studied for molecular switches, logic gates, sensors, molecular machines, and other applications.[2b,5] In covalent TTF–A systems, an appropriate choice of the acceptor and the nature of the linkage are of paramount importance for the modulation of their intramolecular-charge-transfer (ICT) and photophysical properties. The various TTF–acceptor systems that have been described so far have included fused derivatives, such as TTF–dipyridophenazine,[6] TTF–phthalocyanine,[7] TTF–perylenediimide,[8] TTF–TCNQ,[9] and TTF–porphyrins,[10] and derivatives with a direct covalent link between the TTF unit and the acceptor, such as TTF–pyridinium,[11] TTF–oxophenalenoxyl,[12] and TTF–1,3,5-triazine.[13] Although benzothiadiazole (BTD)[14] is an excellent electron-accepting chromophore,[15] which has been used extensively in the construction of materials for red-light emission,[16] organic field-effect transistors (OFETs),[17] photovoltaic cells,[18] and nonlinear optical materials,[19] over the last few decades, it has not so far been associated with a TTF unit. Herein, we describe the synthesis, full characterization, and electrochemical and photophysical studies of two tetrathiafulvalene–benzothiadiazole compounds (TTF–BTD, Scheme 1) that either contain a direct covalent link (**2**) or a fused connection between the two units (**3**), together with theoretical calculations on both systems. Indeed, owing to the different natures of the linkage between the donor (TTF) and acceptor units (BTD) in compounds **2** and **3**, differences in their photophysical properties can be expected.

[a] Dr. F. Pop, Dr. N. Avarvari
LUNAM Université, Université d'Angers
CNRS UMR 6200, Laboratoire MOLTECH-Anjou
2 bd Lavoisier, 49045 Angers (France)
E-mail: narcis.avarvari@univ-angers.fr

[b] A. Amacher, J. Hauser, Dr. S.-X. Liu, Prof. S. Decurtins
Departement für Chemie und Biochemie
Universität Bern, Freiestrasse 3, 3012 Bern (Switzerland)
E-mail: liu@iac.unibe.ch

[c] Dr. J. Ding, Dr. L. M. L. Daku, Prof. A. Hauser, M. Koch
Department of Physical Chemistry, University of Geneva
30 Quai Ernest Ansermet, 1211 Geneva (Switzerland)
E-mail: andreas.hauser@unige.ch

Supporting information for this article is available on the WWW under http://dx.doi.org/10.1002/chem.201202742, including experimental details, characterization of the compounds, X-ray data, photophysical measurements, CV data, and details of the theoretical calculations.

WILEY ONLINE LIBRARY

© 2013 Wiley-VCH Verlag GmbH & Co. KGaA, Weinheim

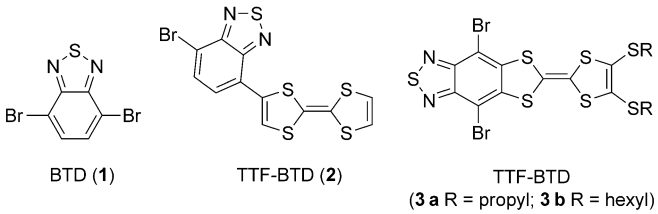

Scheme 1. Structures of the BTD acceptor (**1**) and TTF–BTD D–A systems **2** and **3**.

Results and Discussion

Synthesis and characterization: TTF–BTD **2** was synthesized by a palladium-catalyzed Stille-type coupling reaction between dibromobenzothiadiazole derivative **1** and TTF–$SnMe_3$ (Scheme 2), according to a procedure that has been

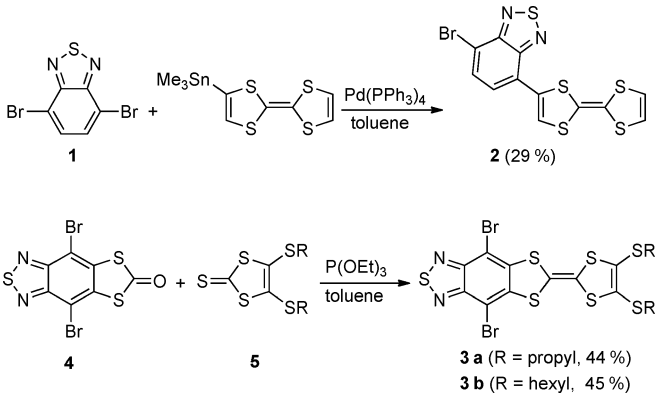

Scheme 2. Synthetic routes to TTF–BTDs **2** and **3**.

successfully employed in the synthesis of other TTF derivatives.[20] With key precursor **4**[21] in hand, the synthesis of TTF–BTD systems **3a** and **3b** was accomplished through triethyl–phosphite-mediated coupling reactions with their corresponding 1,3-dithiole-2-thione derivatives. Good solubility of all of these compounds in common organic solvents allowed their easy purification by using standard chromatographic techniques or crystallization, as well as their full characterization. Notably, the chromatographic purification of compound **2** had to be performed in the dark because it was photosensitive as a solution in air (see the photophysical study). Despite the precautions that were taken during the work-up and, consequently, the fact that compound **2** was analytically pure, trace amounts of a highly luminescent impurity that resulted from the photodecomposition of compound **2** (the structure of which was also determined, see below) were visible in its emission spectra.

Suitable single crystals (as thin needles) for X-ray analysis were grown by slow evaporation from a solution of compound **2** in toluene that was kept in the dark, as well as from a solution of compound **3b** in CH_2Cl_2/*n*-hexane. Compound **2** crystallizes in the monoclinic system, with space

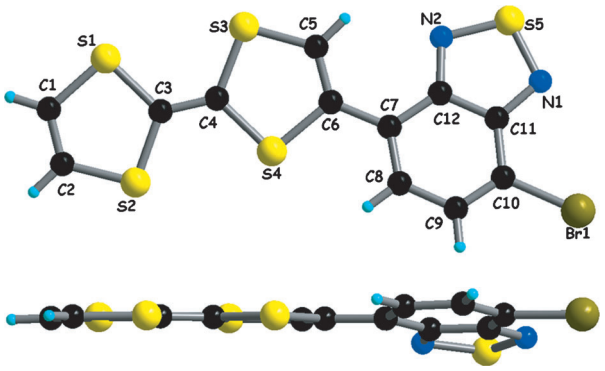

Figure 1. Molecular structure of compound **2** with atom numbering (top).

group $P2_1/n$ and one independent molecule in the unit cell. The dihedral angle between the donor (TTF) and acceptor units (BTD) is 12.5° (Figure 1), whilst the central C=C bond in TTF (1.338(12) Å), together with the C–S bonds, which range between 1.752(9) and 1.773(8) Å, are typical of neutral TTFs. (for more structural parameters, see the Supporting Information, Figure S1 and Table S1).[22,23]

In the single crystals, the molecules form stacks along the *a* direction, with a clear segregation between the donor and acceptor groups (Figure 2); the shortest S···S intermolecular contacts within these stacks are in the range 3.91–3.99 Å. However, short intermolecular N···S (3.12 Å) and Br···S distances (3.62 Å) are observed between molecules, thus forming a layer in the *bc* plane.

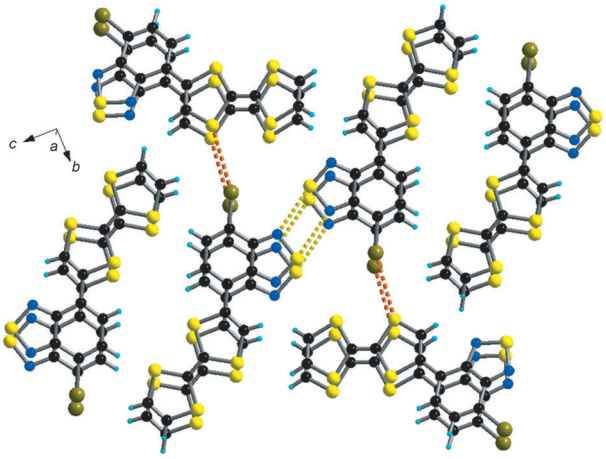

Figure 2. Packing diagram of compound **2**, with an emphasis on short interstacking N···S (S5···N1 (1−*x*, −*y*, 1−*z*), 3.12 Å, yellow) and Br···S interactions (Br1···S3 (0.5−*x*, 0.5+*y*, 0.5−*z*), 3.62 Å, red) in the *bc* plane.

An ORTEP of compound **3b** is shown in Figure 3. Compound **3b** crystallizes as the solvated compound **3b**·*x*C_6H_{14} in the triclinic space group $P\bar{1}$. The asymmetric unit comprises the complete molecule; thus, all of the atoms lie in general positions. The skeleton of the molecule is almost planar; the rms deviation from a least-squares plane through all of the atoms, excluding the two peripheral hexyl groups,

 © 2013 Wiley-VCH Verlag GmbH & Co. KGaA, Weinheim

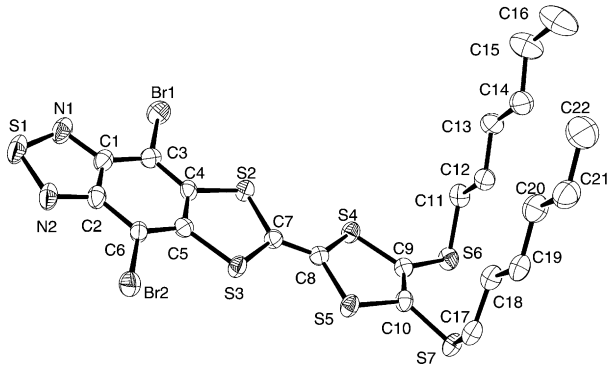

Figure 3. ORTEP of compound **3b**. Ellipsoids are set at 50% probability; hydrogen atoms and solvent molecules have been omitted for clarity. Selected interatomic distances [Å] and angles [°]: C7–C8 1.341(5), C8–S4 1.755(4), C8–S5 1.751(4), C7–S2 1.758(4), C7–S3 1.755(4), C4–C5 1.443(5), C9–C10 1.328(6); S2–C7–S3 115.8(2), S4–C8–S5 114.6(2), C1–C3–C4 119.4(4), C2–C6–C5 117.9(4), C4–S2–C7 96.08(19), C5–S3–C7 95.90(19), C8–S4–C9 94.97(19), C8–S5–C10 95.40(19).

is 0.0378 Å. Similarly, a least-squares plane through the atoms of the TTF core alone reveals a rms deviation of only 0.0373 Å. The bond lengths in the TTF moiety are within the expected range for neutral TTF derivatives.[23] Figure 4

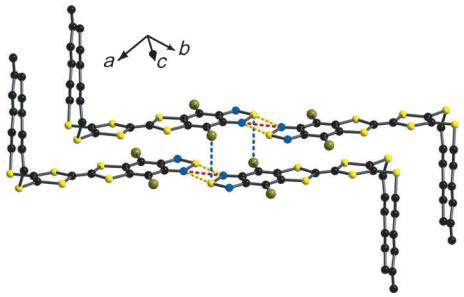

Figure 4. Crystal packing of compound **3b**; hydrogen atoms and solvent molecules have been omitted for clarity.

shows a mutual arrangement of the molecules within the crystal structure, which are oriented approximately parallel to the (132) plane. A noticeable feature is the coplanar head-to-head alignment of pairs of molecules, which are related by a center of inversion with two short intermolecular N···S contacts (3.197 Å) and one short N···N contact (2.927 Å). However, another two Br···S contacts (3.586 Å) are joined to a third molecule, which are again related by an inversion center.

Notably, in both cases, two BTD rings are associated by two antiparallel N···S contacts, thus forming a four-membered cyclic supramolecular synthon, as described in the literature.[24] However, the resulting packing motifs are quite different. For compound **2**, additional Br···S contacts, together with the N···S contacts, result in the formation of 2D layers of the molecules in the *bc* plane. For compound **3b**, the N···S contacts result in a head-to-head dimerization of the BTD units and the weaker Br···S contacts and the presence of hexyl groups result in the formation of continuous slipped stacks, with TTF sitting on top of the BTD unit.

Electrochemistry: Cyclic voltammetry (see the Supporting Information, Figure S2 A, B) of compounds **2**, **3a**, and **3b** show one reversible reduction at −1.19, −1.16, and −1.14 V versus SCE, respectively, which is attributed to the one-electron reduction of the benzothiadiazole moiety (Table 1). As

Table 1. Redox potentials [V] (vs. SCE) of compounds **2** (in CH_2Cl_2/MeCN) and **3** (in CH_2Cl_2).

Compound	$E^{ox1}_{1/2}$	$E^{ox2}_{1/2}$	$E^{red1}_{1/2}$
2	0.42	0.83	−1.19
3a[a]	0.79	1.14	−1.16
3b[a]	0.82	1.16	−1.14

[a] For comparison, potentials were converted into SCE by subtracting 0.04 V from the measured values (vs. Ag/AgCl).

expected, all of these compounds undergo two reversible oxidation processes, which are assigned to the two successive one-electron oxidations of the TTF group. In comparison with compound **2**, compounds **3a** and **3b** exhibit approximately 0.4 V higher oxidation potentials, owing to the strong electronic interactions between the TTF and BTD units, by virtue of a rigid π-conjugated alignment. These results indicate that the HOMO, which is localized on the TTF subunit, is at lower energy in compounds **3a** and **3b** than in compound **2**, owing to the stronger electron-withdrawing effect of the two bromo-substituents, whereas the LUMOs, which are localized on the benzothiadiazole moiety, are at similar energies. This latter result can be rationalized by the fact that, in compound **2**, the donating effect of the TTF unit is compensated for by one electron-withdrawing Br substituent, whereas, in compound **3**, which has a more-efficient conjugation, the stronger electron donation from the TTF unit onto the BTD unit is balanced by the effect of two Br substituents, thus leading to an overall similar effect on the LUMO and, hence, the values of the reduction potentials. Both assumptions are supported by theoretical calculations (see below).

Optical absorption behavior of neutral compounds 2 and 3a: To show the presence of donor-to-acceptor ICT in compounds **2** and **3a**, UV/Vis measurements were performed in solution (Figure 5). In comparison to the absorption spectrum of compound **1**, the absorption spectrum of compound **2** in CH_2Cl_2 shows additional intense absorption bands between 25000 and 35000 cm^{-1} (400–285 nm), which can be ascribed to the TTF unit.[25] These bands arise at similar energies as the $^1\pi\pi^*$ excited states in benzothiadiazole,[26,27] with extinction coefficients (ε) of the order 9.1×10^3 to $1.7\times10^4\,M^{-1}cm^{-1}$. A medium-intense band in the region 13000–23000 cm^{-1} (780–440 nm), with a peak at 17670 cm^{-1} (566 nm) and $\varepsilon = 3.1\times10^3\,M^{-1}cm^{-1}$, can be tentatively attrib-

 © 2013 Wiley-VCH Verlag GmbH & Co. KGaA, Weinheim

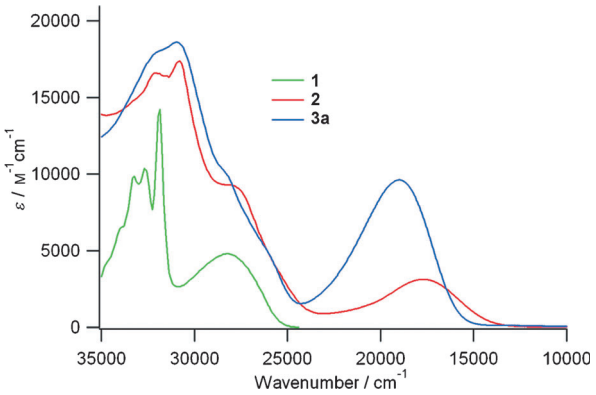

Figure 5. UV/Vis absorption spectra of compounds **1**, **2**, and **3a** in CH_2Cl_2 at room temperature.

uted to a singlet intramolecular charge transfer (^{1}ICT) π-(TTF)→π*(BTD) transition.

Compound **3a** shows similar absorption bands between 25000 and 35000 cm^{-1}, which are likewise ascribed to the $^1\pi\pi^*$ excited states of the TTF and benzothiadiazole units. With $\varepsilon = 1\times10^4\,M^{-1}cm^{-1}$, the ^{1}ICT absorption in the region 15000–25000 cm^{-1} and centered at 18975 cm^{-1} (527 nm) is stronger than that of compound **2**. The increase in absorption is attributed to the rigid π-conjugated alignment of the chromophores in compound **3a**. Consistent with the CV data, the energy of the ^{1}ICT state in compound **3a** is higher than that in compound **2**. The bathochromic shift of the ICT band for compound **2** with respect to compound **3a** is also in agreement with the DFT calculations, which show a larger HOMO–LUMO gap in compound **3a** than in compound **2** (see below).

The high solubility of compound **2** in a variety of organic solvents allowed a detailed study of its solvatochromic behavior (Figure 6). Accordingly, the ^{1}ICT absorption band is slightly blue-shifted on moving from non-polar solvent (cyclohexane, ν_{max} = 17065 cm^{-1}, 586 nm; toluene, ν_{max} = 17450 cm^{-1}, 573 nm) to moderately polar solvent (CH_2Cl_2, ν_{max} = 17670 cm^{-1}, 566 nm; $CHCl_3$, ν_{max} = 17515 cm^{-1}, 570 nm) and highly polar solvent (MeCN, ν_{max} = 18285 cm^{-1}, 547 nm; DMF, ν_{max} = 17985 cm^{-1}, 556 nm), as expected for a ^{1}ICT transition. The overall solvatochromic behavior is less pronounced for compound **3a** (see the Supporting Information, Figure S3), for which the ^{1}ICT absorption band is initially very slightly bathochromically shifted on moving from non-polar solvent (cyclohexane, ν_{max} = 18975 cm^{-1}, 527 nm; toluene, ν_{max} = 19470 cm^{-1}, 514 nm) to moderately polar solvent (CH_2Cl_2, ν_{max} = 18975 cm^{-1}, 527 nm; $CHCl_3$, ν_{max} = 18795 cm^{-1}, 533 nm) and hypsochromically shifted, as expected, only for highly polar solvents (MeCN, ν_{max} = 19645 cm^{-1}, 509 nm; DMF, ν_{max} = 19765 cm^{-1}, 506 nm).[22] This result indicates that the excited-state dipole moment for compound **3** is substantially smaller than that for compound **2**, as expected from the conjugation of the directly fused BTD to TTF.

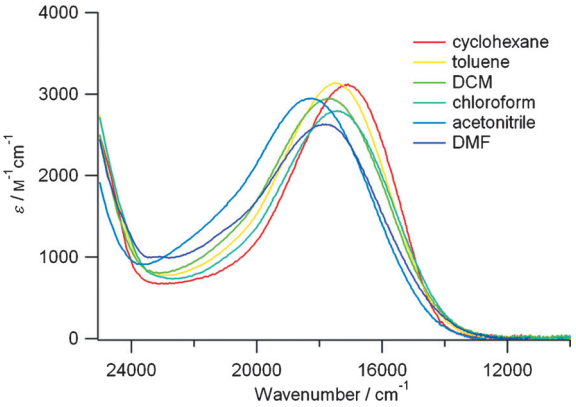

Figure 6. ^{1}ICT absorption band of compound **2** in different solvents at room temperature.

Luminescence behavior of neutral compounds 2 and 3a: In accordance with other substituted BTDs,[26] the precursor (**1**) is emissive in degassed CH_2Cl_2 at room temperature (see the Supporting Information, Figure S4).[22] Upon excitation at ν_{ex} = 28570 cm^{-1} (350 nm), compound **1** shows a broad emission centered at 23260 cm^{-1} (430 nm), which is assigned to the $^1\pi\pi^*$ excited state of the BTD unit.[26,27]

TTF–BTD derivative **2** is also emissive in degassed solutions of various solvents at room temperature. In cyclohexane (see the Supporting Information, Figure S5), the emission apparently strongly depends upon the irradiation wavelength. Irradiation at ν_{ex} = 17240 cm^{-1} (580 nm), that is, into the ^{1}ICT band, results in a broad emission that is centered at 13625 cm^{-1} (734 nm), with a quantum yield of 0.9%. The corresponding excitation spectrum, which is monitored at the emission maximum, is identical to the absorption spectrum. Thus, we can safely conclude that this emission is intrinsic to compound **2** and, accordingly, it is assigned as a ^{1}ICT emission. Excitation at higher energies, such as ν_{ex} = 25000 cm^{-1} (400 nm), results in an emission band at 20410 cm^{-1} (490 nm) and the corresponding excitation spectrum is very different from the absorption spectrum, thus indicating that this emission is more likely to be due to a highly luminescent impurity. This conclusion is further borne out by emission-lifetime measurements (see the Supporting Information, Figure S6A, and the detailed discussion therein). This luminescent impurity, which is present in analytically undetectable amounts in compound **2**, has been determined to be a BTD unit that is connected to a dithiolone moiety (see below), which originates from the aerobic photodecomposition of compound **2** during the work-up. Notably, compound **2** is also weakly emissive in CH_2Cl_2 (see the Supporting Information, Figures S6B and S7) and absorption spectra of both fresh solutions of compound **2** and solutions after a series of measurements are identical, thus indicating that compound **2** is photostable (see the Supporting Information, Figure S8) under anaerobic conditions and under irradiation at energies < 30000 cm^{-1} (> 330 nm). The photophysical data for compound **2** are summarized in Table 2. The emission maximum in CH_2Cl_2 appears at too-high energy because of the non-negligible contribution of

 © 2013 Wiley-VCH Verlag GmbH & Co. KGaA, Weinheim

Table 2. Photophysical data for TTF–BTD systems **2** and **3a** at room temperature.

Compound	Solvent	ν_{abs} [cm^{-1}] (ε [$M^{-1}cm^{-1}$])	ν_{em} [cm^{-1}]	Φ_f	τ [ns]
2	CH_2Cl_2	32045 (16600) 30870 (17400) 27695 (9100) 17670 (3100)	15245[a]	0.0024[a]	0.11(2)[b]
	cyclohexane	32150 (13500) 30775 (13700) 27480 (8000) 17065 (3100)	13625	0.0086	0.35(3)
3a	CH_2Cl_2	32155 (17800) 30960 (18600) 28330 (10100) 18975 (9600)	13550	0.0092	0.87(6)
	cyclohexane	32260 (14200) 31155 (14500) 28250 (7300) 27175 (5200) 25840 (3500) 18795 (9400)	16235	0.014	–

[a] Includes a contribution from an impurity; [b] the lifetime of the fast component is attributed to the emission of compound **2**.

the luminescence of the impurity, even for irradiation at the maximum of the ^{1}ICT band. However, the corresponding lifetime, which is taken as the fastest component in the double exponential fit, corresponds to the intrinsic lifetime of the ^{1}ICT state.

As mentioned above, the photostability of compound **2** is lost in non-degassed solutions and, in air, its absorption and emission spectra change dramatically (see the Supporting Information, Figure S9A). Clearly, the fluorescent impurity that is initially observed in the emission spectra of compound **2** corresponds to a product of aerobic photodegradation, which is subsequently isolated from the complex reaction mixture that results from the exposure of a non-degassed solution of compound **2** to solar irradiation (see the Supporting Information, Figure S9B). The corresponding compound (**6**), which was identified by single-crystal X-ray analysis (it crystallizes in the triclinic space group $P\bar{1}$), ^{1}H NMR spectroscopy, and MS (see the Supporting Information, Figure S10 and Table S2), is a BTD–dithiolone that is formally derived from the oxidative cleavage of the central C=C bond of TTF. This type of photodegradation reaction has previously been seen in a Ru^{II} complex of a TTF–phenanthroline ligand.[28]

Compound **3a** is weakly emissive in non-polar or moderately polar solvents. In cyclohexane (Figure 7a), the emission maximum upon excitation at $\nu = 18870\ cm^{-1}$ (530 nm) is at $16235\ cm^{-1}$ (616 nm), with a quantum efficiency of 1.4%. This emission is gradually red-shifted on increasing the polarity of the solvent, whilst, at the same time, its intensity decreases (Figure 7b). The excitation spectra for this emission are identical to the absorption spectra in the region of the ^{1}ICT band in cyclohexane, as well as in CH_2Cl_2 (see the Supporting Information, Figure S11).[22] Therefore, we may safely conclude that this emission comes exclusively

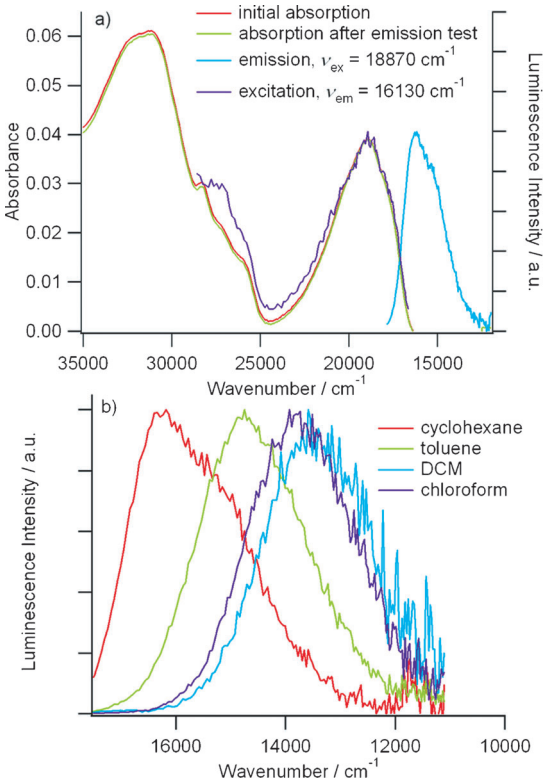

Figure 7. a) Absorption, emission, and excitation spectra of compound **3a** in cyclohexane ($c = 4\times10^{-6}$ M) at room temperature; b) emission spectra of compound **3a** in different solvents ($\nu_{ex} = 18870\ cm^{-1}$).

from compound **3a**. For the latter solvent, the quantum efficiency is 0.9% and the corresponding luminescence-decay time is 0.87(6) ns (Figure 8). Furthermore, the photodecomposition of compound **3a** is slow, so this compound can be considered to be stable when exposed to light, even in the presence of oxygen. These luminescence lifetimes and quantum yields are consistent with a radiative lifetime that corresponds to the oscillator strength of the broad absorption

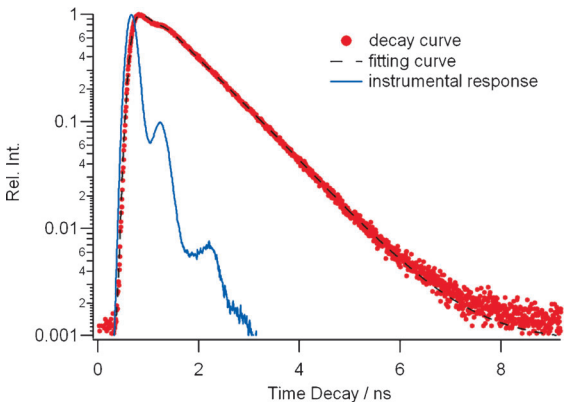

Figure 8. Emission decay of compound **3a** in CH_2Cl_2 by using a KC18 (680 nm) cut-off filter, excitation: $20000\ cm^{-1}$, detection: $13800\ cm^{-1}$ (725 nm). The lifetime was determined by a mono-exponential fit by using a convolution fitting procedure; instrument response (blue), experimental data (red), and mono-exponential fit (dashed line).

© 2013 Wiley-VCH Verlag GmbH & Co. KGaA, Weinheim

band that is centered at 18870 cm^{-1} (530 nm). Therefore, together with the red shift of the emission with increasing solvent polarity, we may safely conclude that the first excited and luminescent state of compound **3a** is an ICT state. The photophysical data for compound **3** are collected in Table 2.

Photophysical study of oxidized compounds 2 and 3a: The evolution of the absorption spectrum of compound **2** after oxidation by $FeCl_3$ in CH_2Cl_2 at room temperature is shown in Figure 9. Although quasi-immediate and quantitative oxidation is observed, the new intense absorption bands between 20000 and 25000 cm^{-1} and between 14000 and 20000 cm^{-1} indicate the formation of the radical cation $TTF^{+\bullet}$.[25] The same spectroscopic evolution is observed upon chemical oxidation with $NOBF_4$, as well as electrochemically (see the Supporting Information, Figure S12 A, B). In addition to the changes in the spectroscopic region from 12000 to 26000 cm^{-1}, marked changes, masked by the absorption bands of $FeCl_3$, are also observed at higher energies. In particular, the strong absorption band with a peak at 32000 cm^{-1} is bleached upon oxidation, thus corresponding to bleaching of the $^1\pi\pi^*$ transitions of the neutral TTF unit. Whereas chemical oxidation with $FeCl_3$ leads to an oxidized form of compound **2** that is stable in solution for at least 1 h, oxidation with $NOBF_4$ is followed by chemical degradation within about 10 min (see the Supporting Information, Figure S13 A, B), which precludes the use of this oxidizing agent for further luminescence studies. However, the one-electron-oxidized species of compound **2** in degassed CH_2Cl_2 did not show any additional luminescence, except for the luminescence that was previously attributed to a BTD-type impurity (see the Supporting Information, Figure S14).

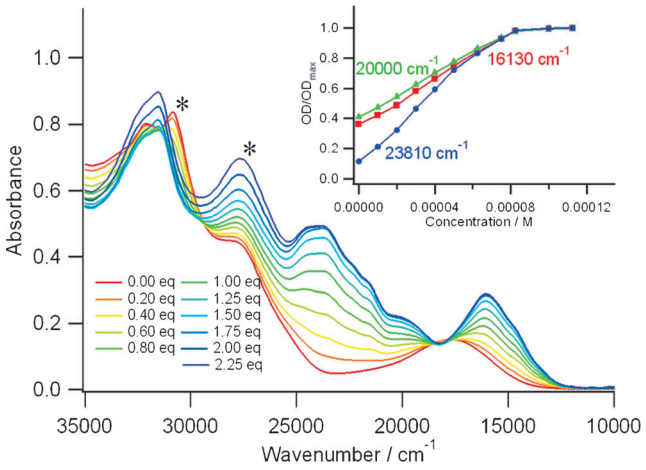

Figure 9. UV/Vis absorption spectra of compound **2** during chemical oxidation by the successive addition of $FeCl_3$ as an oxidant in CH_2Cl_2 at room temperature. Inset: Change in absorbance at different wavenumbers in compound **2** by the successive addition of $FeCl_3$; * denotes unreacted $FeCl_3$.

The chemical oxidation of compound **3a** has to be performed with $NOBF_4$ because the redox potential of $FeCl_3$ is too low. The corresponding evolution of the absorption spectrum of compound **3a** with the successive addition of $NOBF_4$ in CH_2Cl_2 at room temperature is shown in Figure 10. Quantitative oxidation is observed, but not instantaneously. The oxidation process is comparatively slow and takes about 1 h to proceed to completion if three equivalents of $NOBF_4$ are added in one portion (see the Supporting Information, Figure S15 A). The new absorption bands that are centered at 23000 and 12000 cm^{-1} indicate the formation of the radical cation $TTF^{+\bullet}$.[25] On the basis of previous observations[6a] and quantum-mechanical calculations (see below), this latter result can be ascribed to an ICT transition in the opposite direction to that of the neutral species, that is, from benzothiadiazole to $TTF^{+\bullet}$. In the case of compound **3a**, the oxidized species is relatively stable, even after oxidation with $NOBF_4$ for 30 min.[22] The electrochemical oxidation of compound **3a** in CH_2Cl_2 at room temperature[22] results in a spectroscopic evolution that is consistent with the chemical oxidation study (see the Supporting Information, Figure S15 B).

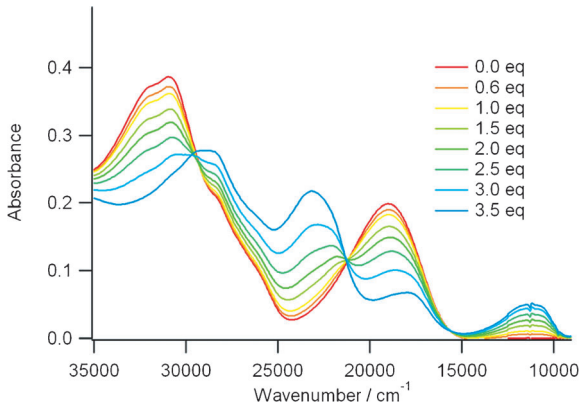

Figure 10. UV/Vis absorption spectra of compound **3a** during chemical oxidation by the addition of $NOBF_4$ as an oxidant in CH_2Cl_2 at room temperature.

The one-electron-oxidized species of compound **3a** in CH_2Cl_2 at room temperature shows weak luminescence at 16100 cm^{-1} (see the Supporting Information, Figure S16). The corresponding excitation spectrum is comparable to the absorption spectrum between 17000 and 30000 cm^{-1}, which, in principle, allows the identification of this emission as intrinsic to the one-electron-oxidized species of compound **3a**. However, at this stage, it is very difficult to assign this emission, because it does not correspond to emission from the lowest excited state.

DFT calculations: To substantiate these assignments and the orbital nature of the electronic transitions for compounds **2** and **3a**, theoretical calculations[29] were performed at the DFT/PBE level[30] for geometry optimizations and at the TDDFT/PBE0[31] level for electronic excitations. All calcula-

 © 2013 Wiley-VCH Verlag GmbH & Co. KGaA, Weinheim

tions were performed by using the Gaussian 09 program package.[32]

The ground-state geometry of compound **2** was optimized with no symmetry constraints, starting from the experimentally observed X-ray structure. The resulting conformation of the equilibrium geometry shows a slight deviation from planarity and the bond lengths and angles are in good agreement with the experimental geometry (see the Supporting Information, Figure S17).[22] In particular, the calculated dihedral angle between the TTF and BTD units (4°) is in good agreement with the experimental value (12.5°); this latter value is somewhat larger owing to packing forces. The calculated C=C and C–S bond lengths, 1.359 and 1.766/1.779 Å, respectively, are also close to the experimental values (1.338 and 1.752/1.773 Å). In agreement with the donor and acceptor character of the TTF and BTD units, respectively, the π-type HOMO is localized on the former group, whereas the π-type LUMO is rather low in energy (−3.024 eV) and is spread over the entire benzothiadiazole moiety (Figure 11 a).

Notable are the π-type HOMO−1, with contributions from both units, and LUMO+1 orbitals, which are involved in the main low-energy transitions (see below), as well as the value of the HOMO–LUMO gap (2.07 eV). Vertical excitations were calculated on the optimized ground-state geometry of compound **2** at the time-dependent DFT level.[22] Accordingly, the lowest-energy singlet transition, which was predicted to be at 12580 cm^{-1} (795 nm), with an oscillator strength of $f=0.097$, corresponds to a $\pi_{HOMO}\rightarrow\pi^*_{LUMO}$ transition, thus clearly indicating an intramolecular CT transition from the TTF donor to the BTD acceptor (see the Supporting Information, Table S3). The next intense transitions S_3 (23193 cm^{-1}, 431 nm, $f=0.084$) and S_4 (25160 cm^{-1}, 397 nm, $f=0.112$) are very close in energy to each other and consist of combinations of HOMO−1→LUMO and HOMO→LUMO+1 transitions; the former transition mainly corresponds to a $^1\pi\pi^*$ excitation of the BTD unit. The Supporting Information, Figure S19 shows an overlay of the calculated spectrum of compound **2** (as a stick plot) with the experimental spectrum.

The DFT-optimized ground-state geometry of neutral compound **3** is in full agreement with the experimentally determined structure, including the deviation from planarity of the TTF unit. In comparison, the optimized structure of the one-electron-oxidized species only shows very small deviations from planarity, as demonstrated by the overlay of the two structures in Figure 12.

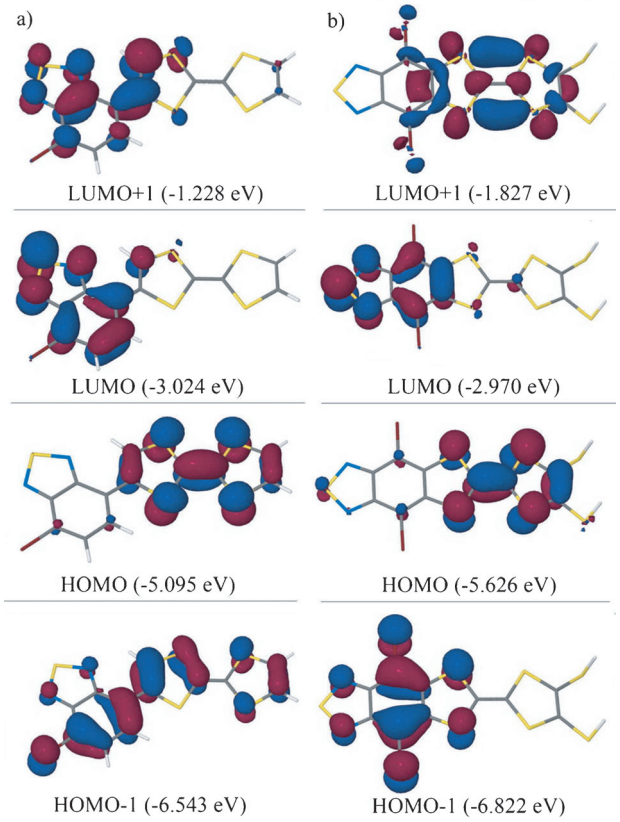

Figure 11. Frontier orbitals for the neutral forms of compounds: a) **2** and b) **3** that are involved in the $S_0\rightarrow S_n$ transitions. For a complete presentation of the molecular orbitals and optical transitions, see the Supporting Information, Figures S18 and S21, and Tables S3 and S4.

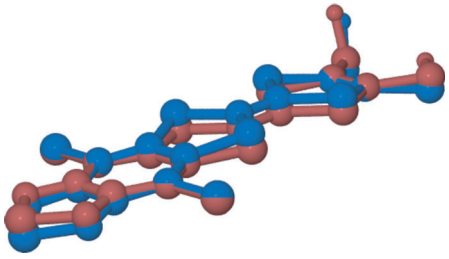

Figure 12. Ground-state geometries of neutral (blue) and oxidized (red) compound **3** (the alkyl groups refer to methyl groups) optimized at the DFT/PBE level (also see the Supporting Information, Figure S20).

As observed for compound **2**, the HOMO and LUMO of neutral compound **3** are localized on the TTF and BTD units, respectively (Figure 11 b and the Supporting Information, Figure S21). Also, the experimental spectrum of the neutral species of compound **3** can be satisfactorily analyzed on the basis of TDDFT calculations. An inspection of the contributions to the various $S_0\rightarrow S_n$ transitions (see the Supporting Information, Table S4) reveals that, in particular, the lowest excited state of the neutral species corresponds to an almost pure intramolecular $S_0\rightarrow S_1$ CT from the HOMO (localized on TTF) to the LUMO (localized on the BTD unit). In comparison to compound **2**, the corresponding oscillator strength is almost three-times higher, in accordance with the experimental data, and, with a HOMO–LUMO gap of 2.66 eV (compared to 2.07 eV for compound **2**), this result is also in accordance with the higher energy of the ICT transition and the higher oxidation potential for compound **3** compared to compound **2**. On the other hand,

 © 2013 Wiley-VCH Verlag GmbH & Co. KGaA, Weinheim

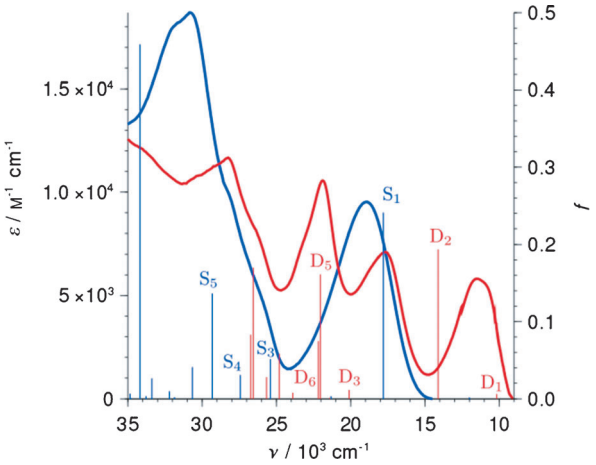

Figure 13. Comparison of the experimental (line graph) and calculated absorption spectra (stick plot) of neutral (blue) and one-electron-oxidized compound **3** (red).

the intense, higher-energy $S_0 \rightarrow S_3$ and $S_0 \rightarrow S_4$ transitions correspond to $^1\pi\pi^*$ transitions that are localized on the BTD and TTF moieties, respectively. Figure 13 shows the experimental spectrum overlaid by the calculated spectrum as a stick plot. A key feature of both spectra is a well separated, low-energy absorption band.

For the one-electron-oxidized species of compound **3**, the singly occupied molecular orbital (SOMO) corresponds to the α-HOMO and the β-LUMO is localized on the TTF unit, which, in accordance with electrochemical data, corresponds to a $TTF^{+\bullet}$ radical (Figure 14). Likewise, the lowest-energy excited state of the one-electron-oxidized species of compound **3** corresponds to an intramolecular charge transfer, but, this time, from the HOMO (localized on BTD) to the SOMO (on the $TTF^{+\bullet}$ radical), or, more precisely, to a $D_0 \rightarrow D_1$ transition from the β-HOMO to the β-LUMO (see the Supporting Information, Table S5). However, the more intense band that corresponds to the $D_0 \rightarrow D_2$ transition at slightly higher energy corresponds to a β-HOMO−1→β-LUMO transition, with the β-HOMO−1 delocalized over both subunits of the radical cation. Higher-energy transitions correspond to transitions of mixed character and $^1\pi\pi^*$ transitions that are localized on the BTD unit. Figure 13 includes an overlay of the calculated spectrum (as a stick plot) with the experimental spectrum. Even though the agreement between the experimental and calculated spectra is not as good as for the neutral species, it satisfactorily reproduces the key features.

Analogous calculations on the oxidized form of compound **2** (see the Supporting Information, Figure S23A, B and Table S6) reveal that its lowest-energy absorption band also corresponds to an ICT transition from the BTD unit to the $TTF^{+\bullet}$ radical.

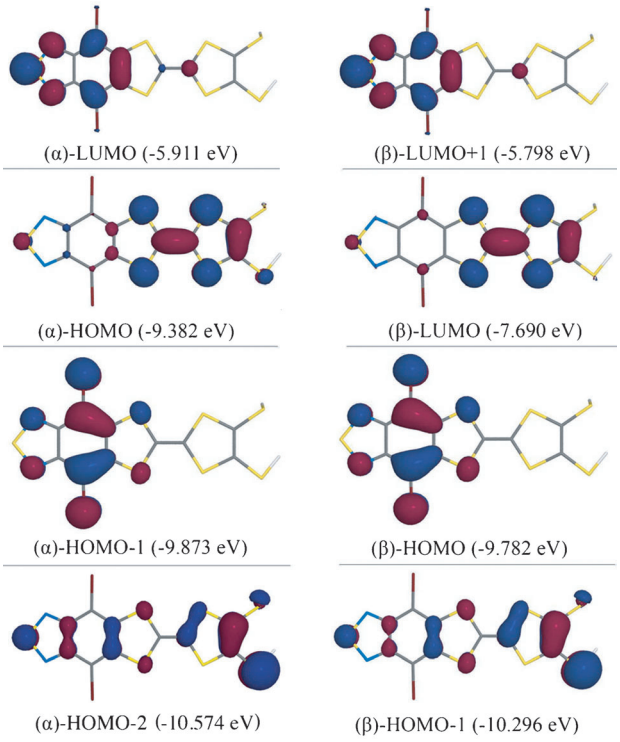

Figure 14. Frontier orbitals of one-electron-oxidized compound **3** that are involved in the $D_0 \rightarrow D_n$ transitions. For a complete presentation of the molecular orbitals and $D_0 \rightarrow D_n$ transitions, see the Supporting Information, Figures S22 A and B, and Table S5.

Conclusion

Two covalently linked donor–acceptor systems (**2** and **3**), which contain tetrathiafulvalene (TTF) donor and benzothiadiazole (BTD) acceptor units, have been synthesized and fully characterized, including by single-crystal X-ray diffraction (for compounds **2** and **3b**). All of these systems show a lowest-energy transition that corresponds to the ^{1}ICT π(TTF)→π*(BTD) excited state. Upon excitation into the ICT state, they show emission. Owing to the better overlap of the HOMO and LUMO in the fused scaffold of compound **3**, the intensity of the ^{1}ICT band is substantially higher compared to that in compound **2**. This better overlap also accounts for higher oxidation potential for compound **3** than for compound **2**, which, in turn, results in a higher energy of the ^{1}ICT transition for compound **3** and clearly impacts on its photochemical stability. Even though both compounds are photostable in de-oxygenated solution, compound **2** readily degrades in the presence of oxygen under 254 nm UV light or in sunlight. Chemical and electrochemical oxidation lead to the formation of the radical cation ($TTF^{+\bullet}$). Notably, upon oxidation of compound **3a**, the converse ICT transition, that is, benzothiadiazole→$TTF^{+\bullet}$, has been observed in the near-IR region, as predicted by DFT calculations. Whereas the emission properties of the neutral compounds present some similarities in the sense that the emission bands originate from the ICT bands, their energies,

 © 2013 Wiley-VCH Verlag GmbH & Co. KGaA, Weinheim

lifetimes, and efficiencies are quite different. Moreover, the oxidized species of compound **3a** is still luminescent, whilst in structure $\mathbf{2}^{+\bullet}$, the luminescence is completely quenched.

This study was driven by the search for donor–acceptor systems with optimized absorption properties and charge-transfer states in the visible and near-IR regions, along with improved photochemical stabilities. Tuning the substitution pattern of the donor unit in the covalently linked system should allow for the modulation of its oxidation potential and, possibly, of its photostability. The concept of annulation of TTF directly onto acceptor units holds promise for future development, for instance with regard to photoconductivity studies of these molecules that are adsorbed onto surfaces or embedded in conductive polymers, as well as for the construction of organic dyes for high efficiency solar-energy conversion.

Experimental Section

General: Reactions were carried out under an argon atmosphere in toluene (HPLC grade). NMR spectra were recorded on Bruker Avance DRX 500 (500.04 MHz for ^{1}H, 125 MHz for ^{13}C) and Bruker Avance DRX 300 spectrometers (300 MHz for ^{1}H, 75 MHz for ^{13}C). Chemical shifts are expressed in parts per million, downfield from TMS as an external reference. The following abbreviations are used: singlet (s), doublet (d), triplet (t), sextet (st), multiplet (m). MS (MALDI-TOF) spectra were recorded on a Bruker Biflex-IIITM that was equipped with a 337 nm N2 laser. HRMS (ESI) data were obtained on a Thermo Scientific LTQ Orbitrap XL in positive mode. Elemental analysis was recorded on a Flash 2000 Fisher Scientific Thermo Electron Analyzer.

Synthesis of TTF–BTD 2: 4,7-Dibromo-2,1,3-benzothiadiazole (587 mg, 2 mmol), 2-(trimethylstannyl)tetrathiafulvalene (245 mg, 0.66 mmol), and $[Pd(PPh_3)_4]$ as catalyst (120 mg, 5% mmol) were mixed in dry toluene (20 mL) and heated at reflux for 12 h under an argon atmosphere. The mixture was filtered through Celite and silica gel, washed with toluene and CH_2Cl_2. The combined organic phases were evaporated and purified by column chromatography on silica gel (CH_2Cl_2/*n*-hexane, 4:1 then 1:1) to give a black solid. Yield: 80 mg (29%); ^{1}H NMR (500 MHz, CD_2Cl_2): $\delta = 8.19$ (s, 1H), 7.42 (d, ^3J(H,H) = 8.0 Hz, 1H), 7.27 (d, ^3J(H,H) = 7.5 Hz, 1H), 6.40 ppm (s, 2H); ^{13}C NMR (125 MHz, CD_2Cl_2): $\delta = 154.2$, 151.9, 132.7, 131.1, 128.5, 124.7, 124.3, 124.2, 119.7, 113.9 ppm; MS (MALDI-TOF): *m/z* calcd for $C_{12}H_5BrN_2S_5$: 415.82; found: 415.90; elemental analysis calcd. (%) for $C_{12}H_5BrN_2S_5$: C 34.53, H 1.21, N 6.71; found: C 34.16, H 1.24, N 6.40.

Synthesis of TTF–BTD 3a: 4,8-Dibromo[1,3]dithiolo[4,5-*f*]-2,1,3-benzothiadiazol-6-one (1.09 g, 2.84 mmol) and 4,5-bis(propylthio)-1,3-dithiole-2-thione (905 mg, 3.20 mmol) were added into a microwave vial (capacity: 10–20 mL). Dry toluene (6 mL) and triethylphosphite (7 mL) were added and the solution was degassed by bubbling through argon gas for 10 min. Then, the solution was heated in an oil bath for 5 min at 130 °C. The solution was poured into MeOH (100 mL), filtered, and rinsed with copious amounts of MeOH. The product was purified by column chromatography on silica gel (CH_2Cl_2/*n*-hexane, 1:1). Yield: 0.77 g (44%); ^{1}H NMR (300 MHz, $CDCl_3$): $\delta = 2.83$ (t, $J = 7.22$ Hz, 4H), 1.69 (st, $J = 7.27$ Hz, 4H), 1.04 ppm (t, $J = 7.33$ Hz, 6H); ^{13}C NMR (75 MHz, $CDCl_3$): $\delta = 206.8$, 144.1, 128.1, 103.0, 38.4, 30.9, 23.2, 13.2 ppm; MS (ESI): *m/z* calcd for $C_{16}H_{14}Br_2N_2S_7$: 615.7563; found: 615.7545.

Synthesis of TTF–BTD 3b: 4,8-Dibromo[1,3]dithiolo[4,5-*f*]-2,1,3-benzothiadiazol-6-one (600 mg, 1.56 mmol) and 4,5-bis(hexylthio)-1,3-dithiole-2-thione (859 mg, 2.34 mmol) were added into a microwave vial (capacity: 10–20 mL). Dry toluene (8 mL) and triethylphosphite (10 mL) were added and the solution was degassed by bubbling through argon gas for 10 min. Then, the solution was then heated in an oil bath for 5 min at 90 °C. The solution was poured into MeOH (150 mL), filtered, and rinsed with copious amounts of MeOH. The product was purified by column chromatography on silica gel (CH_2Cl_2/*n*-hexane, 1:2). Yield: 0.49 g (45%); ^{1}H NMR (300 MHz, $CDCl_3$): $\delta = 2.85$ (t, $J = 7.33$ Hz, 4H), 1.65 (m, 4H), 1.38 (m, 12H), 0.90 ppm (t, $J = 6.90$, 6H); MS (ESI): *m/z* calcd for $C_{22}H_{26}Br_2N_2S_7$: 699.8502; found: 699.8491.

X-Ray structure determination: Details regarding data collection and solution refinement are given in Table 3. X-ray diffraction measurements for compounds **2** and **6** were performed on a Bruker Kappa CCD diffractometer in an X-ray tube with a graphite monochromator ($Mo_{K\alpha}$ radiation, $\lambda = 0.71073$ Å). The structures were solved (SHELXS-97) by using direct methods and refined (SHELXL-97) by full-matrix least-square procedures on F^2.[33] All non-H atoms were refined anisotropically. Hydrogen atoms were introduced at calculated positions (riding model) and were included in the structure-factor calculations but not refined. The crystals of compounds **2** and **6** were very thin needles; therefore, the data sets were only of medium quality.

Table 3. Crystallographic data, details of data collection, and structure-refinement parameters of compounds **2**, **3b**, and **6**.

	2	**3b**	**6**
formula	$C_{12}H_5BrN_2S_5$	$C_{22}H_{26}Br_2N_2S_7$	$C_9H_3BrN_2OS_3$
M_w [g mol^{-1}]	417.39	702.69	331.22
T [K]	293(2)	173(2)	293(2)
crystal system	monoclinic	triclinic	triclinic
space group	$P2_1/n$	$P\bar{1}$	$P\bar{1}$
a [Å]	3.9920(2)	5.41856(12)	4.0669(19)
b [Å]	22.364(3)	16.2836(3)	11.499(19)
c [Å]	16.384(2)	16.9824(4)	11.821(17)
α [°]	90.00	99.5460(18)	98.26(12)
β [°]	93.475(7)	91.1122(18)	92.05(6)
γ [°]	90.00	92.4393(18)	97.52(8)
V [Å^3]	1460.0(3)	1475.80(5)	541.5(12)
Z	4	2	2
ρ_{calcd} [g cm^{-3}]	1.899	1.581	2.031
μ [mm^{-1}]	3.518	3.257	4.348
GOF on F^2	1.099	1.116	1.056
final R_1/wR_2 [$I > 2\sigma(I)$]	0.0809/0.1965	0.0479/0.0934	0.0970/0.2367
R_1/wR_2 (all data)	0.1134/0.2096	0.0697/0.0992	0.1613/0.2757

A crystal of compound **3b** was mounted with Paratone onto a glass needle and used for X-ray structure determination at −100 °C. All measurements were made on an Oxford Diffraction SuperNova area-detector diffractometer1 by using mirror optics ($Mo_{K\alpha}$ radiation, $\lambda = 0.71073$ Å). The unit-cell constants and an orientation matrix for data collection were obtained from a least-squares refinement of the setting angles of 10240 reflections within the range $1.60 < \theta < 28.15°$. A total of 2832 frames were collected by using ω scans, a 20 s exposure time, a rotation angle of 0.5° per frame, and a crystal-detector distance of 65.0 mm. Data reduction was performed by using the CrysAlisPro[34] program. The intensities were corrected for Lorentz and polarization effects and an absorption correction, based on the multi-scan method, by using SCALE3 ABSPACK in CrysAlisPro[34] was applied. Data collection and refinement parameters are given in Table 3. The structure was solved by using direct methods with SIR97,[35] which revealed the positions of all non-hydrogen atoms in the host. The non-hydrogen atoms were refined anisotropically. All hydrogen atoms were placed at geometrically calculated positions and refined by using a riding model, in which each H-atom was assigned a fixed isotropic displacement parameter with a value that was equal to 1.2 Uequiv of its parent atom (1.5 Uequiv for methyl groups). The remaining electron density in the solvent-accessible voids was accounted for by using the SQUEEZE technique in program PLATON.[36] Refinement of the structure was carried out on F^2 by using full-matrix least-squares techniques, which minimized the function $\Sigma w(F_o^2 - F_c^2)^2$. The weighting scheme was based on counting statistics and included a factor

 © 2013 Wiley-VCH Verlag GmbH & Co. KGaA, Weinheim

to downgrade the intense reflections. All calculations were performed by using the SHELXL-97[37] program.

Electrochemical studies: Cyclic voltammetry (CV) measurements of compound **2** were performed inside a glove box, which contained dry, oxygen-free (<1 ppm) argon gas, by using a three-electrode cell that was equipped with a platinum millielectrode (area: 0.126 cm^2), a Ag/Ag^+ pseudo-reference electrode, and a platinum-wire counter electrode. The potentials were re-adjusted with respect to the saturated calomel electrode (SCE). The electrolyte was a 0.1 M solution of $(n-Bu_4N)PF_6$ in THF. All of the experiments were performed at RT at a scan rate of 0.1 $V s^{-1}$. The experiments were performed on an EGG PAR 273A potentiostat with positive feedback compensation.

CV analysis of compounds **3a** and **3b** was performed in a three-electrode cell that was equipped with a Pt-disk working electrode, a glassy carbon counter electrode, and a Ag/AgCl reference electrode. The electrochemical experiments were carried out under a dry and oxygen-free atmosphere in CH_2Cl_2, with $(n-Bu_4N)PF_6$ (0.1 M) as a supporting electrolyte. The voltammograms were recorded on a PGSTAT 101 potentiostat.

Photophysical studies: CH_2Cl_2, MeCN, cyclohexane, toluene, and DMF (the best available quality) for the photophysical and electrochemical analysis were purchased from commercial sources and used as received without further purification. UV/Vis absorption spectra were measured on a Cary 5000 spectrophotometer. Steady-state emission spectra were recorded on a Fluorolog 3 spectrophotometer. Fluorescence-lifetime measurements were performed on a custom-built time-correlated photon-counting system by using a pulsed diode laser at a frequency of 1 MHz. The preparation of samples in different solvents and given concentrations started from a standard solution in concentrated CH_2Cl_2. The proportion of CH_2Cl_2 in the final solution was less than 5% (v/v) in all of the tested samples.

Samples in solution with proper concentrations were prepared by optical dilution for steady-state photoluminescence (OD < 0.1) spectroscopy and most samples were deoxygenated for 30 min in a quartz cell (path length: 1 cm) prior to measurements by bubbling with N_2 gas. Precautions were taken to limit the exposure of the photosensitive complexes to light in between measurements and during bubbling.

Theoretical calculations: All calculations were performed with the Gaussian 09 program package.[32] Geometry optimization was carried out with the PBE functional[30] and the TDDFT[31a] electronic excitation calculations were carried out with the PBE1PBE (i.e., PBE0) functional.[31c] The atoms were described by using Dunning's correlation-consistent basis sets augmented with diffuse functions,[38] namely the aug-cc-pVDZ basis set for the H atoms and the aug-cc-pVTZ basis set for the C, N, S, and Br atoms.

Acknowledgements

Financial support from the CNRS, the University of Angers, the National Agency for Research (ANR, Project No. 09-BLAN-0045-01), and the Swiss National Science Foundation (Grant Nos. 200020-137567 and 200020-130266) is gratefully acknowledged.

[1] J.-L. Brédas, D. Beljonne, V. Coropceanu, J. Cornil, *Chem. Rev.* **2004**, *104*, 4971–5004.
[2] a) J. L. Segura, N. Martin, *Angew. Chem.* **2001**, *113*, 1416–1455; *Angew. Chem. Int. Ed.* **2001**, *40*, 1372–1409; b) D. Canevet, M. Sallé, G. X. Zhang, D. Q. Zhang, D. B. Zhu, *Chem. Commun.* **2009**, 2245–2269.
[3] a) M. R. Bryce, *Adv. Mater.* **1999**, *11*, 11; b) M. Bendikov, F. Wudl, D. F. Perepichka, *Chem. Rev.* **2004**, *104*, 4891–4945.
[4] J. O. Jeppesen, M. B. Nielsen, J. Becher, *Chem. Rev.* **2004**, *104*, 5115–5131.
[5] A. R. Pease, J. O. Jeppesen, J. F. Stoddart, Y. Luo, C. P. Collier, J. R. Heath, *Acc. Chem. Res.* **2001**, *34*, 433–444.
[6] a) C. Jia, S.-X. Liu, C. Tanner, C. Leiggener, A. Neels, L. Sanguinet, E. Levillain, S. Leutwyler, A. Hauser, S. Decurtins, *Chem. Eur. J.* **2007**, *13*, 3804–3812; b) C. Goze, C. Leiggener, S.-X. Liu, L. Sanguinet, E. Levillain, A. Hauser, S. Decurtins, *ChemPhysChem* **2007**, *8*, 1504–1512; c) N. Dupont, Y.-F. Ran, H.-P. Jia, J. Grilj, J. Ding, S.-X. Liu, S. Decurtins, A. Hauser, *Inorg. Chem.* **2011**, *50*, 3295–3303.
[7] C. Loosli, C. Jia, S.-X. Liu, M. Haas, M. Dias, E. Levillain, A. Neels, G. Labat, A. Hauser, S. Decurtins, *J. Org. Chem.* **2005**, *70*, 4988–4992.
[8] M. E. El-Khouly, M. Jaggi, B. Schmid, C. Blum, S.-X. Liu, S. Decurtins, K. Ohkubo, S. Fukuzumi, *J. Phys. Chem. C* **2011**, *115*, 8325–8334.
[9] F. Otón, V. Lloveras, M. Mas-Torrent, J. Vidal-Gancedo, J. Veciana, C. Rovira, *Angew. Chem.* **2011**, *123*, 11094–11098; *Angew. Chem. Int. Ed.* **2011**, *50*, 10902–10906.
[10] H. Jia, B. Schmid, S.-X. Liu, M. Jaggi, P. Monbaron, S. V. Bhosale, S. Rivadehi, S. J. Langford, L. Sanguinet, E. Levillain, M. E. El-Khouly, Y. Morita, S. Fukuzumi, S. Decurtins, *ChemPhysChem* **2012**, *13*, 3370–3382.
[11] a) O. Paz-Tal Levi, J. Y. Becker, A. Ellern, V. Khodorkovsky, *Tetrahedron Lett.* **2001**, *42*, 1571–1573; b) Q.-Y. Zhu, Y. Liu, W. Lu, Y. Zhang, G.-Q. Bian, G.-Y. Niu, J. Dai, *Inorg. Chem.* **2007**, *46*, 10065–10070.
[12] S. Nishida, Y. Morita, K. Fukui, K. Sato, D. Shiomi, T. Takui, K. Nakasuji, *Angew. Chem.* **2005**, *117*, 7443–7446; *Angew. Chem. Int. Ed.* **2005**, *44*, 7277–7280.
[13] a) F. Riobé, P. Grosshans, H. Sidorenkova, M. Geoffroy, N. Avarvari, *Chem. Eur. J.* **2009**, *15*, 380–387; b) D. G. Branzea, A. Fihey, T. Cauchy, A. El-Ghayoury, N. Avarvari, *Inorg. Chem.* **2012**, *51*, 8545–8556.
[14] K. R. J. Thomas, J. T. Lin, M. Velusamy, Y.-T. Tao, C.-H. Chuen, *Adv. Funct. Mater.* **2004**, *14*, 83–90.
[15] M. Akhtaruzzaman, M. Tomura, J. Nishida, Y. Yamashita, *J. Org. Chem.* **2004**, *69*, 2953–2958.
[16] C. T. Chen, *Chem. Mater.* **2004**, *16*, 4389–4400.
[17] a) Md. Akhtaruzzaman, N. Kamata, J. Nishida, S. Ando, H. Tada, M. Tomura, Y. Yamashita, *Chem. Commun.* **2005**, 3183–3185; b) J. Zaumseil, C. L. Donley, J.-S. Kim, R. H. Friend, H. Sirringhaus, *Adv. Mater.* **2006**, *18*, 2708–2712; c) T. Kono, D. Kumaki, J. Nishida, T. Sakanoue, M. Kakita, H. Tada, S. Tokito, Y. Yamashita, *Chem. Mater.* **2007**, *19*, 1218–1220; d) M. Zhang, H. N. Tsao, W. Pisula, C. Yang, A. K. Mishra, K. Müllen, *J. Am. Chem. Soc.* **2007**, *129*, 3472–3473.
[18] a) M. Velusamy, K. R. J. Thomas, J. T. Lin, Y. Hsu, K. Ho, *Org. Lett.* **2005**, *7*, 1899–1902; b) Z.-M. Tang, T. Lei, K.-J. Jiang, Y.-L. Song, J. Pei, *Chem. Asian J.* **2010**, *5*, 1911–1917.
[19] K. R. J. Thomas, A. L. Thompson, A. V. Sivakumar, C. J. Bardeen, S. Thayumanavan, *J. Am. Chem. Soc.* **2005**, *127*, 373–383.
[20] F. Riobé, N. Avarvari, P. Grosshans, H. Sidorenkova, T. Berclaz, M. Geoffroy, *Phys. Chem. Chem. Phys.* **2010**, *12*, 9650–9660.
[21] H.-P. Jia, J. Ding, Y.-F. Ran, S.-X. Liu, C. Blum, I. Petkova, A. Hauser, S. Decurtins, *Chem. Asian J.* **2011**, *6*, 3312–3321.
[22] CCDC-886354 (**2**), CCDC-891310 (**3b**), and CCDC-905008 (**6**) contain the supplementary crystallographic data for this paper. These data can be obtained free of charge from The Cambridge Crystallographic Data Centre via www.ccdc.cam.ac.uk/data_request/cif.
[23] a) S.-X. Liu, S. Dolder, E. B. Rusanov, H. Stoeckli-Evans, S. Decurtins, *C. R. Acad. Sci. Paris Chimie* **2003**, *6*, 657–662; b) T. Devic, N. Avarvari, P. Batail, *Chem. Eur. J.* **2004**, *10*, 3697–3707.
[24] A. F. Cozzolino, I. Vargas-Baca, S. Mansour, A. H. Mahmoudkhani, *J. Am. Chem. Soc.* **2005**, *127*, 3184–3190.
[25] P. R. Ashton, V. Balzani, J. Becher, A. Credi, M. C. T. Fyfe, G. Mattersteig, S. Menzer, M. B. Nielsen, F. M. Raymo, J. F. Stoddart, M. Venturi, D. J. Williams, *J. Am. Chem. Soc.* **1999**, *121*, 3951–3957.
[26] a) T. Ishi-I, N. Nakamura, N. Esaki, S. Amemori, *Chem. Lett.* **2008**, *37*, 1166–1167; b) D. Aldakov, M. A. Palacios, P. Anzenbacher, Jr., *Chem. Mater.* **2005**, *17*, 5238–5241.
[27] B. Da Silveira Neto, A. Lopes, G. Ebeling, R. Goncalves, V. Costa, F. Quina, J. Dupont, *Tetrahedron* **2005**, *61*, 10975–10982.

 © 2013 Wiley-VCH Verlag GmbH & Co. KGaA, Weinheim

[28] L. K. Keniley, Jr., L. Ray, K. Kovnir, L. A. Dellinger, J. M. Hoyt, M. Shatruk, *Inorg. Chem.* **2010**, *49*, 1307–1309.
[29] a) P. Hohenberg, W. Kohn, *Phys. Rev.* **1964**, *136*, B864–B871; b) W. Kohn, L. J. Sham, *Phys. Rev.* **1965**, *140*, A1133–A1138.
[30] a) J. P. Perdew, K. Burke, M. Ernzerhof, *Phys. Rev. Lett.* **1996**, *77*, 3865–3868; b) J. P. Perdew, K. Burke, M. Ernzerhof, *Phys. Rev. Lett.* **1997**, *78*, 1396–1396.
[31] a) M. E. Casida, *Time-Dependent Density Functional Response Theory for Molecules, in Recent Advances in Density Functional Methods* (Ed.: D. P. Chong), World Scientific, Singapore, **1995**; b) K. Burke, M. Ernzerhof, J. P. Perdew, *Chem. Phys. Lett.* **1997**, *265*, 115–120; c) C. Adamo, V. Barone, *J. Chem. Phys.* **1999**, *110*, 6158–6169.
[32] Gaussian 09, Revision C.01, Gaussian, Inc., Wallingford CT, **2010**, for a full list of authors see the Supporting Information.
[33] G. M. Sheldrick, *Programs for the Refinement of Crystal Structures*, University of Göttingen, Göttingen, Germany, **1996**.
[34] Oxford Diffraction, CrysAlisPro (Version 1.171.34.36). Oxford Diffraction Ltd., Yarnton, Oxfordshire, UK, **2010**.
[35] A. Altomare, G. Cascarano, C. Giacovazzo, A. Guagliardi, M. C. Burla, G. Polidori, M. Camalli, *SIR92, J. Appl. Crystallogr.* **1994**, *27*, 435–436.
[36] A. L. Spek, *J. Appl. Crystallogr.* **2003**, *36*, 7–13.
[37] G. M. Sheldrick, *Acta Crystallogr. Sect. A* **2008**, *64*, 112–122.
[38] a) T. H. Dunning, Jr., *J. Chem. Phys.* **1989**, *90*, 1007–1023; b) D. E. Woon, T. H. Dunning, Jr., *J. Chem. Phys.* **1993**, *98*, 1358–1471.

Received: July 30, 2012
Published online: January 4, 2013

 © 2013 Wiley-VCH Verlag GmbH & Co. KGaA, Weinheim